Article

Intermittent Very High Frequency Plasma Deposition on Microcrystalline Silicon Solar Cells Enabling High Conversion Efficiency

Mitsuoki Hishida [1],*, Takeyuki Sekimoto [2], Mitsuhiro Matsumoto [3] and Akira Terakawa [3]

[1] Automotive & Industrial Systems Company, Panasonic Corporation, Kadoma, Osaka 571-8506, Japan
[2] Advanced Research Division, Panasonic Corporation, Seika, Kyoto 619-0237, Japan;
     sekimoto.takeyuki@jp.panasonic.com
[3] Eco Solution Company, Panasonic Corporation, Kaizuka, Osaka 597-0094, Japan;
     matsumoto.mi@jp.panasonic.com (M.M.); terakawa.akira@jp.panasonic.com (A.T.)
* Correspondence: hishida.mitsuoki@jp.panasonic.com; Tel./Fax: +81-50-3380-2095 (ext. 2308)

Abstract: Stopping the plasma-enhanced chemical vapor deposition (PECVD) once and maintaining the film in a vacuum for 30 s were performed. This was done several times during the formation of a film of i-layer microcrystalline silicon (µc-Si:H) used in thin-film silicon tandem solar cells. This process aimed to reduce defect regions which occur due to collision with neighboring grains as the film becomes thicker. As a result, high crystallinity (X_c) of µc-Si:H was obtained. Eventually, a solar cell using this process improved the conversion efficiency by 1.3% (0.14 points), compared with a normal-condition cell. In this paper, we propose an easy method to improve the conversion efficiency with PECVD.

Keywords: thin-film silicon tandem solar cell; microcrystalline silicon; amorphous silicon; crystallinity; plasma-enhanced chemical vapor deposition; conversion efficiency

1. Introduction

Stable high quality hydrogenated microcrystalline silicon (µc-Si:H) films which are used in thin-film silicon tandem solar cells have been difficult to make since the quality of µc-Si:H varies depending on its underlying shape or film thickness [1]. This is because a defective component in the µc-Si:H film is affected by transparent conductive oxide (TCO) texture, as the film thickness of the microcrystalline silicon increases [2]. To avoid a defective region being formed and achieve high conversion efficiency (*Eff*), the surface morphology of TCO was modified to have a blunt angle or rounded shape [3]. Recently, École Polytechnique Fédérale de Lausanne has developed thin-film silicon solar cells with 12.63% efficiency [4]. Also, as the current maximum value of *Eff*, the National Institute of Advanced Industrial Science and Technology (AIST) reported the *Eff* of 12.69% with a triode plasma-enhanced chemical vapor deposition (PECVD) reactor [5].

As a model of a defective region generated, when µc-Si:H is grown from the slope of the texture shape of TCO, a defective region ingenerates at the collided point of each µc-Si:H [6,7]. A defective region is affected by the underlying shape or the underlying film quality. It has been reported that the defective region consists of vacancies and a low-density amorphous region [2]. Previously, we proposed another factor for the formation of a defective region due to the shadowing effect on incident radicals [2], which should reduce the X_c [8].

Beyond that, a defective region also occurs with the continuous deposition film after becoming thicker. This defect region was caused by colliding with the neighboring grains after the film become

thicker [9]. This is because μc-Si:H grows perpendicular to the textured substrate. The reduction in X_c was revealed by micro-crystallinity depth profiling measurements [8,10]. An X_c profiling technique was reported by Choong *et al.* who measured the X_c profiling of the early-stage (<800 nm) of μc-Si:H. Therefore, in this report, we aim to reduce the collisions with the neighboring grains by stopping the PECVD once to make the epitaxial μc-Si:H film thinner (>1000 nm). Finally, a high conversion efficiency solar cell can be expected. Since the beginning period of discharge is an unstable process, the value of X_c can be expected to decrease if epitaxial growth of μc-Si:H is halted by temporarily stopping the PECVD. Impurities which come from the deposition chamber also influence the quality of μc-Si:H.

As a comparative experiment to reduce the defective region correlating to the film thickness gain, an experiment was carried out. The experimental method is very simple; the plasma-discharge of very high frequency (VHF) PECVD should be stopped once and then the chamber with a vacuum is held for a few seconds (although this process stopped the epitaxial growth of μc-Si:H, this experimental method is referred to as "*SEG*"). In the actual experiment, *SEG*, which was done twice or three times, produces an equal thickness during the i-layer deposition. For ease of evaluating *SEG*, all samples were deposited with pulsed-PECVD [11]. This is because the pulsed-PECVD can be expected to reduce the ion-bombardment and short lifetime species [12,13]. Using a different *SEG* method, characteristic improvement was reported by Urbain *et al.* [14]. Even though they used a different way of profiling the controlled SiH_4, the aim of suppressing the reduction of X_c was the same as that of the *SEG* experiments. In only the experiment where *SEG* was done twice using the thin-film silicon tandem solar cells, this X_c of test cells became higher than that of normal-condition cells, and it did not decrease during the process of forming a thick film as well as the case using X_c-adjustment layer [8]. Eventually, *Eff* improved by 1.3% (0.14 points), V_{oc} by 0.011 V, and *FF* by 0.002 compared with those for the normal-condition cell.

2. Experimental Methods

In this study, actual thin-film silicon tandem solar cells were used for the evaluation of *SEG*. The structure of these cells was glass/tin oxide (SnO_2)/a-Si:H (p-i-n)/μc-Si:H (p-i-n)/back electrode [15]. For TCO, a commercial SnO_2-based TCO substrate (Asahi VU, Asahi Glass, Tokyo, Japan) was adopted. μc-Si:H and a-Si:H were deposited by plasma-enhanced chemical vapor deposition (PECVD).

Typically, when the μc-Si:H is deposited with PECVD, the plasma-discharge power is not stopped before reaching the target thickness. However, in this study, when the thickness reached one-third of t (t/3) and two-thirds of t (2t/3), *SEG* was done twice, if the total thickness of i-μc-Si:H is t (=2300 nm). The evacuation times of *SEG* were carried out in two modes: 30 s and 600 s, and these were labeled cells A and B, respectively. This degree of vacuum was under 5×10^{-3} (pa). The vacuum time of 30 s was determined by the time required for the deposition gases (SiH_4/H_2) to me almost completely eliminated from the chamber. It is due to a return to the default deposition position. The impact of long time exposure of the cell to the vacuum chamber was compared with that for the cell with the 600 s exhaust time (B cells). Only the difference between cell A and cell B influences the impurities while discharge is halted. The structures of a normal-condition cell and a cell made using the *SEG* cell (cells A and B) are shown in Figure 1.

Additionally, different numbers of *SEG* experiments were carried out simultaneously. Since X_c is correlated with the film thickness, the value of X_c changes according to the number of *SEG*. When the thickness reached one-fourth of t (t/4), two-fourths of t (2t/4), and three-fourths of t (3t/4), *SEG* was done three times, if the total thickness of i-μc-Si:H is t (=2300 nm). One evacuation time of *SEG* was 30 s, which is the same as for cell A. This was labeled cell C. The degree of vacuum was under 5×10^{-3} (pa), which is the same as for cells A and B. Table 1 summarizes these conditions.
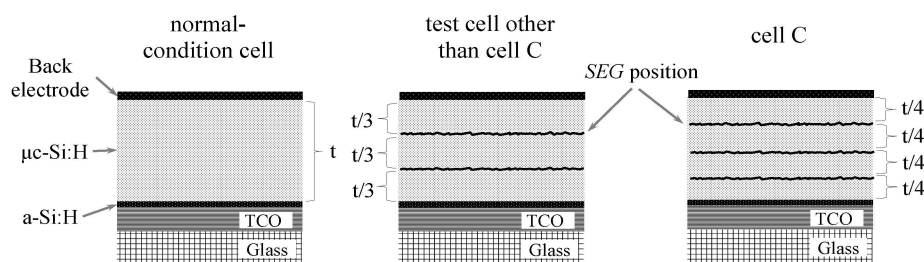
Figure 1. Cell structure comparison between normal-condition, *SEG* (other than cell C) and a *SEG* cell (cell C). The i-μc-Si:H thicknesses were t. *SEG* was done when the thicknesses reached t/3 and 2t/3, t/4, 2t/4, and 3t/4.

Table 1. Comparison of i-μc-Si:H thickness constitution with normal-condition cells A, B and C; as well as normal-condition film and films A. One time of evacuations times of *SEG*, and total evacuations times of that with films A and cells A, B and C.

Description	Normal Condition Cell/Film	Cell A/Film A	Cell B	Cell C
i-layer constitution	t	t/3 + t/3 + t/3		t/4 + t/4 + t/4 + t/4
total i-later thickness		t (=2300 nm)		
exhaust time between i-layer (s)	0	30	600	30
total exhaust time (s)	0	60	1200	90

The cell position and temperature of the heater were maintained during *SEG*. After the *SEG*, the same gases as the deposition conditions were supplied for 30 s, and then plasma-dischargewas restarted again. The total discharge time of μc-Si:H was the same for the whole duration of these experiments, although the discharge was stopped during the deposition. All the μc-Si:H treatment times with PECVD became longer by only around 5 min, except for cell B.

Furthermore, to verify the reproducibility of the *SEG* process, two other types of *SEG* tests were carried out. These test conditions were different from the conditions applied to cells A to C, such as the top layer and i-μc-Si:H. However, the *SEG* processes were carried out twice, the same as for cell A. The total thicknesses of i-μc-Si:H were 1500 and 1750 nm: these were labeled cells D and E, respectively. For cell D, the deposition conditions (thickness, gases, power and pressure) of i-μc-Si:H and the top layer condition were varied compared to other cells. Cell E was subjected to conditions different from those applied to cells A to D. The no-*SEG* cells were fabricated simultaneously, and were labeled as having been fabricated under the same normal conditions as those for cell D and cell E. Table 2 summarizes these conditions.

Table 2. Comparison of different i-μc-Si:H thickness (1500/1750 nm) *SEG* processes with cell D and normal-condition cell D, and cell E and normal-condition cell E. Single evacuation times of *SEG* and total exhaust time of cell.

Description	Normal Condition (D)	Cell D	Normal Condition (E)	Cell E
i-layer constitution	t	t/3 + t/3 + t/3	t	t/3 + t/3 + t/3
total i-later thickness		t (=1500 nm)		t (=1750 nm)
exhaust time between i-layer (s)	0	30	0	30
tolal exhaust time (s)	0	60	0	60

The thickness of the i-layer (a-Si:H) in the top layer was sufficient at 240 nm. This was to ensure that the top layer current would have no effect on the bottom layer current, since the bottom layer current has a rate-controlling effect on I_{sc}.

For each condition test, five to eight cells were fabricated. The active area of each cell was 1 cm^2. The I–V characteristics of open circuit voltage (V_{oc}), short circuit current (I_{sc}), fill factor (*FF*), and conversion efficiency (*Eff*) were measured using a solar simulator under an air mass of 1.5 (AM 1.5) at 25 °C.

Pulsed PECVD was used at all times during the i-µc-Si:H process. As the pulsed PECVD conditions, a PECVD frequency of 40 MHz, a pulse modulation frequency of 30 kHz, and a duty ratio of 50% were adopted for i-layer deposition.

For the comparison of X_c, actual normal-condition and cell A cells were used in the analysis with a polishing method. This method was reported in [8]. The actual cell A was analyzed by secondary ion mass spectrometry (SIMS) [16]. Nitrogen and oxygen were analyzed through to the glass substrate from the back electrode side of the cell. SIMS measurementing conditions were as follows: Equipment: CAMECA ims5f (CAMECA, Gennevilliers Cedex, France) Ion conditions: Cs+, 14.5 keV, approximately 30 nA; Measuring area: approximately 30 µm diameter; Depth: calibration by Si sputtering.

In addition to the evaluation of cells, µc-Si:H films have been analyzed simultaneously. In the film evaluations, Eagle XG (Corning, NY, USA) was used as the substrate. A 20 nm p-layer was first deposited on a bare substrate under the same conditions as the cell. Then, two types of process (normal-condition and *SEG*) were carried out at the same thicknesses as for the cell, and these were labeled as normal-condition film and film A. The total µc-Si:H thickness of the normal-condition film and film A were "t", in the same manner as for the cell. For film A, when the thickness reached one-third of t (t/3) and two-thirds of t (2t/3), *SEG* processes were done in the same manner as for cell A. The evacuation time of the *SEG* of film A was 30 s. The i-µc-Si:H films of the normal-condition film and the film A were compared. Table 1 summarizes the conditions.

These two types of film (normal-condition film and film A) were analyzed by Raman spectrometry and Fourier transform infrared spectroscopy (FTIR). The quality of the µc-Si:H film was different from that of a cell because it is affected by the underlying shape. This evaluation was a relative comparison among the films. To distinguish the crystallinity of the cell expressed by "X_c" the crystallinity of the film is referred to as "X_c'". The crystallinity of µc-Si:H was evaluated using a 514 nm wavelength and a Via Reflex Raman microscope (Renishaw, Gloucestershire, UK). The crystallinity evaluated by Raman spectroscopy was defined as $X_c = I_{520}/I_{480}$, where the peak heights of I_{480} and I_{520} are the wavenumbers of 480 and approximately 520 cm^{-1}, respectively [17,18]. Fourier transform infrared spectroscopy (FTIR) measurements using the attenuated total reflection (ATR) method were carried out using a Spectrum 100 instrument (PerkinElmer, Waltham, MA, USA) [19]. The following stretching modes (SM) of Si–H bonds were used to fit the IR spectra: oxide silicone (O_ySiH_x) at about 2250 cm^{-1}, high SM (HSM) at 2100 cm^{-1}, middle SM (MSM) at 2040 cm^{-1}, low SM (LSM) at 2000 cm^{-1}, and extremely low SM (ELSM) at 1925 and 1895 cm^{-1} [20–22]. Each SM was analyzed using the Gaussian mode [23], and each SM fraction was defined as the ratio of the total area of all SMs divided by that SM's area. The LSM was used in the discussion section of this study. The two ELSM values were also simply expressed as ELSM.

3. Results

3.1. Comparison of Conversion Efficiency with the SEG Process Cell

Test results for the cells A–C are shown in Figure 2 and Table 3. Each of the values of *Eff*, V_{oc}, I_{sc}, and *FF* in Table 3 was the average for each condition. The error bars are also the standard deviation (δ) calculated for every condition. All results for the cells (five cells) are plotted in Figure 2. For cell A, *Eff* improved by 1.3% (0.14 points), V_{oc} by 0.011 V, I_{sc} by 0.0021, and *FF* by 0.002 compared with those for the normal-condition cell. The improved I_{sc} and *FF* were within a standard deviation range. Simply performing *SEG* thus improved the *Eff*, V_{oc}, I_{sc}, and *FF*.

For cell B, which has the extended vacuum time, *Eff* improved by 1.1% (0.12 points), V_{oc} by 0.008 V, I_{sc} by 0.08 mA compared with those for the normal-condition cell. This result shows that *SEG* has similar effect to that of cell A. However, no added benefit of *Eff* is obtained by extending the vacuum

time. However, I_{sc} was higher than that for cells prepared under other conditions. The longer the vacuum time is, the higher the I_{sc} available is, but the value of the changed I_{sc} resembled the standard deviation range. The result of *FF* was within the margin of error.
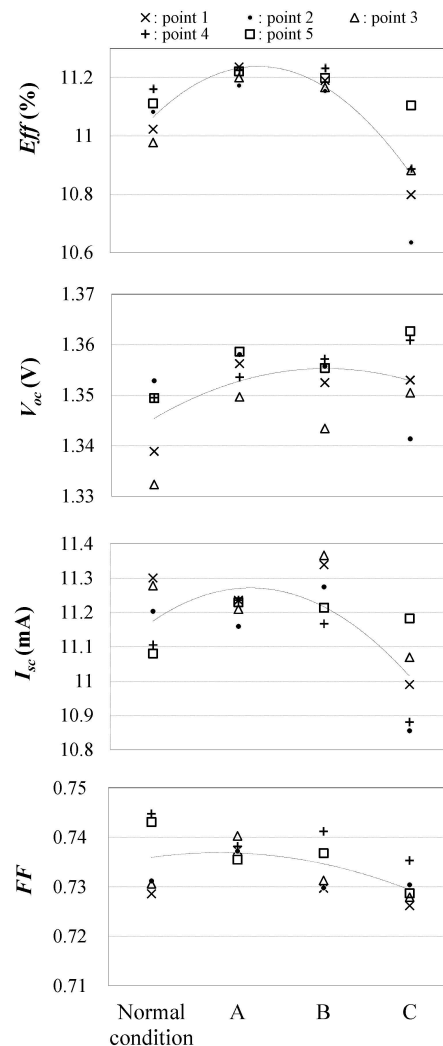

Figure 2. Results of each test cell: normal-condition cell, cell A, cell B, and cell C. For each cell type, five cells were fabricated. Points 1-5 were cells location of substrate.

Table 3. Results for each test cell. Each of the values of *Eff*, V_{oc}, I_{sc}, and *FF* was averaged for each condition. Error bars are standard deviation (δ) calculated for each condition.

	Normal-Condition Cell	**Cell A**	**Cell B**	**Cell C**
V_{oc} (V)	1.345 ± 0.008	1.355 ± 0.003	1.353 ± 0.005	1.354 ± 0.008
I_{sc} (mA)	11.194 ± 0.089	11.214 ± 0.029	11.272 ± 0.074	10.996 ± 0.121
FF	0.736 ± 0.007	0.738 ± 0.002	0.734 ± 0.005	0.730 ± 0.003
Eff (%)	11.07 ± 0.06	11.21 ± 0.02	11.19 ± 0.03	10.86 ± 0.15

For cell C, which increased the number of *SEG* treatments to three, *Eff* decreased by 1.8% (0.21 points), I_{sc} by 0.20 mA compared with those for the normal-condition cell. Although V_{oc} improved by 0.008 V, it was not better than for cell A. At this time of the experiment, two *SEG* trials are better than three trials.

Test results for cells D and E are shown in Table 4 and Figure 3. For cell D, *Eff* increased by 13.1% (1.14 points), I_{sc} by 1.33 mA, *FF* by 0.005 compared with the normal-condition cell D. However,

V_{oc} decreased by 0.027 V. For cell E, *Eff* increased by 2.1% (0.21 points), V_{oc} by 0.006, I_{sc} by 0.31 mA compared with the normal-condition cell E. But increases of V_{oc} and I_{sc} were within a standard deviation range. However, *FF* decreased by 0.009.

Table 4. Results for each test of cell D and cell E. Each of the values of *Eff*, V_{oc}, I_{sc}, and *FF* was averaged for each condition. Normal condition of D is without *SEG*. Normal condition of E is without *SEG*. Error bars are standard deviation (δ) calculated for each condition.

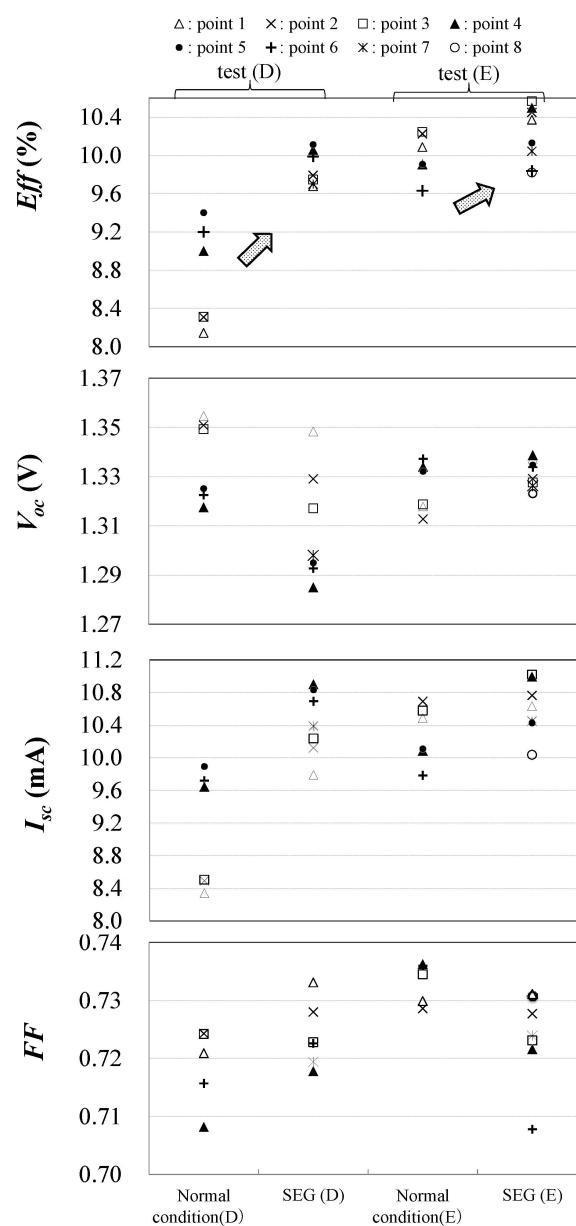|	Normal Condition (E)	Cell D	Normal Condition (D)	Cell E
V_{oc} (V)	1.337 ± 0.015	1.309 ± 0.021	1.325 ± 0.009	1.331 ± 0.005
I_{sc} (mA)	9.099 ± 0.660	10.424 ± 0.380	10.289 ± 0.320	10.597 ± 0.306
FF	0.718 ± 0.01	0.724 ± 0.00	0.7335 ± 0.00	0.724 ± 0.007
Eff (%)	8.72 ± 0.49	9.87 ± 0.167	10.00 ± 0.213	10.21 ± 0.278

Figure 3. Results of each test cell: cell D, cell E, normal-condition cell D, and normal-condition cell E. For each cell type, eight cells were fabricated. Points 1-8 were cells location of substrate.

The results for the all I–V characteristics are relative to the bottom cell condition, because the thickness of the i-layer (a-Si:H) of the top layer is sufficient. For cell B, for which the thickness of the i-layer on top is 240 nm, the J_{sc} values of the top layer and bottom layer were 11.59 and 11.31 mA/cm^2, respectively, assuming external quantum efficiency (EQE). For cell D, for which the thickness of the top i-layer is 240 nm, the J_{sc} values of the top layer and bottom layer were 11.12 and 9.38 mA/cm^2, respectively, with external quantum efficiency. The bottom layer current has a rate-controlling effect on J_{sc}, because a top i-layer thickness of 240 nm was adequate.

3.2. Analysis Results of Actual Crystallinity Profile of µc-Si:H along with Depth

The Raman analysis results of actual crystallinity profiles of the normal-condition cell and the cell A are shown in Figure 4. The relationship between the film thickness and X_c is shown from the µc-Si:H thickness of zero. The obtained figure was plotted from the TCO side, and it also includes the thickness of the p-layer. This is because the p-layer of the bottom cell was µc-Si:H, but its thickness was very small (20 nm). The values of X_c were normalized by the maximum value of X_c among the normal-condition cell and the cell A.
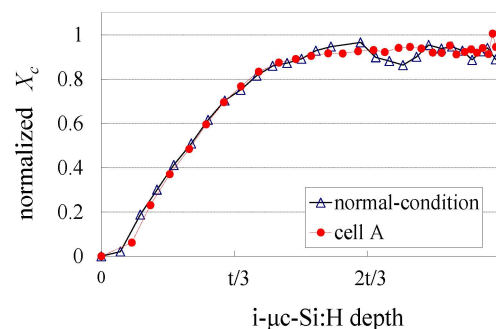

Figure 4. Results of Raman analysis of polished test cells; normal-condition cell and cell A. Values of X_c were normalized by the maximum value of X_c among normal-condition cell and cell A. X_c was expressed from the TCO side.

Both the X_c values did not show any difference between the normal-condition cell and the cell A up to the half thickness (t/2) of µc-Si:H. However, X_c of the normal-condition cell decreased at an around 2t/3. This decrease in X_c was probably caused by a defective region produced after the film thickness increased [8]. These decreases in the values of X_c were measured at four points successively. The values of X_c are connected smoothly, unlike the surrounding values. These decreases in X_c are therefore not due to measurement error. The decreasing X_c during the formation of a thick film inhibited the high X_c of µc-Si:H and effected the *Eff*.

Conversely, there was no reduction in X_c in the thickness direction with cell A. It means that *SEG* has prevented the defective region. In addition, X_c increased with the increasing film thickness, and a maximum X_c was confirmed. In the comparison of the X_c profiles between the normal-condition cell and cell A, *SEG* yielded high values of X_c.

3.3. Secondary Ion Mass Spectrometry Analyses with Cell

Nitrogen impurity levels were analyzed with the normal-condition cell and the cell A shown in Figure 5. Since it was analyzed from the back-contact side by SIMS, the results were expressed in the direction reverse to the deposition direction. In the no *SEG* region of µc-Si:H, nitrogen was detected by about 2.5×10^{18} (atom/cm^3). Nitrogen increased by approximately 10%–15% (about 2.9×10^{18} (atom/cm^3)) in the layers of the *SEG* region: at t/3 and 2t/3. In comparison, under normal conditions, it did not change significantly during the i-layer deposition. Nitrogen gas was never been used at all even after the deposition process in the process chamber. This nitrogen was brought form outside air by the

substrate of the cell or film, or was released as degassing from the wall of the deposition chamber. Nitrogen gas was incorporated into the μc-Si:H [24].
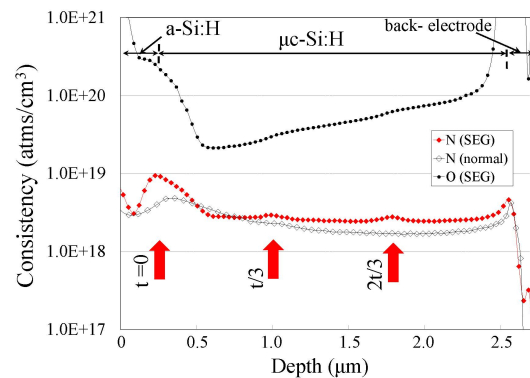

Figure 5. Profile of impurities about nitrogen and oxygen in cell A which used the *SEG* by SIMS. The nitrogen profile for normal-condition cells is also shown. Results were expressed in the direction reverse to the deposition direction.

On the one hand, between the a-Si:H layer and the μc-Si:H layer, nitrogen was detected with a threefold increase (1.0×10^{19} atom/cm^3) compared to other layers of μc-Si:H. When the processing equipment was changed from a-Si:H process to μc-Si:H process, cells were at once exposed to the atmosphere.

Oxygen impurity levels were analyzed with the cell A shown in Figure 5. Slightly more was detected in the *SEG* region of μc-Si:H in the same way as nitrogen. This was caused by the *SEG*. However, a difference level comparison between the *SEG* layer and no *SEG* layer was not as high as for nitrogen. The details are not noted here because the differences were negligible.

3.4. Film Analysis with FTIR and Raman

As a comparison of the normal-condition film and film A, the results of analysis by Raman spectrometry and FTIR are shown in Figure 6. The value of X_c' was normalized by a maximum value of film A.
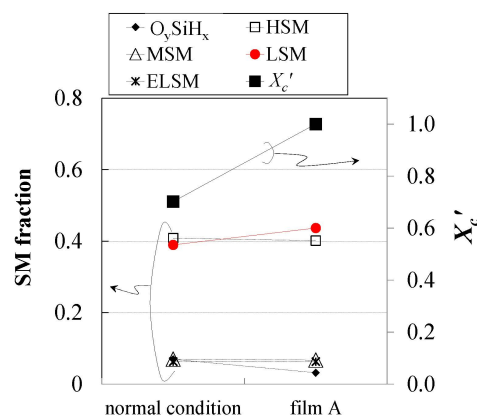

Figure 6. Analyzed results of film tests, normal-condition film and film A, by Raman spectrometry and FTIR. The values of X_c' were normalized by the value of the film A.

The film quality was different from the quality of the cell because that was deposited on the flat-glass rather than textured-TCO. The difference was spread significantly by the flat substrate. Thus, this confirmation was a relative comparison.

In film A, the LSM value was detected as stronger compared to a normal-condition film. This means that the film A contains a large amount of silicon monohydride (Si–H), so this component is expected to

terminate the dangling bonds in μc-Si:H [25]. Also, $O_y SiH_x$ which means crystalline grain boundaries was fewer than in the normal-condition film [19]. Owing to the *SEG*, the quality of μc-Si:H became better on the evaluation of the film.

However, X_c' of film A was higher than that of the normal condition film. The higher X_c', higher LSM, and lower $O_y SiH_x$ of i-μc-Si:H such as film A can yield a high solar cell *Eff*. Thus, *SEG* successfully improved the μc-Si:H quality.

4. Discussion

To reduce the defective region correlation with the film thickness gain, the *SEG* process was carried out. Under its influence, as seen in Figure 4, X_c of μc-Si:H does not decrease the value of X_c during the process of forming a thick film. As a result, the cell achieved a high X_c and the value of X_c' increased. Also, as seen in Figure 6, the LSM value was detected as stronger than in a normal-condition film. Increasing the amorphous component such as LSM improved the quality of μc-Si:H by terminating the dangling bonds in μc-Si:H [26,27]. Eventually, the *Eff*, V_{oc}, and *FF* of cell A improved.

On the other hand, the difference between cell A and cell B, which was the test of discharge stop time, increased the I_{sc}. This characteristic difference was led not only by the initial discharge instability, but also by the impurity incorporation. Nitrogen and oxygen were also detected on the *SEG* cell with SIMS. On another hand, the X_c of μc-Si:H is changed by nitrogen, according to Ehara [28]. In our study of film A, the LSM which corresponds to the amorphous component (Si–H) was increased using the *SEG* layer. From this circumstantial evidence, it is reasonable to assume that nitrogen, which comes from the *SEG* process, increased the amorphous component. More nitrogen in cell B increases the N donor in the amorphous component and may increase the charged Si dangling bonds [29] and finally increased the I_{sc} more than cell A. Or oxygen was increased by *SEG* impurities in the growing film [30].

After the *SEG*, the amorphous component was deposited in the precursor defective region. The crystalline direction of μc-Si:H, which grows perpendicular to the textured substrate, was changed by the amorphous component [31]. As a result, collisions with the neighboring grains were reduced. The oxide might have influenced the X_c as well as nitrogen [32]. On the another front, a large amount of nitrogen was detected in the earlier thickness stage of μc-Si:H (around t = 0) in Figure 5. In exactly the same way, the value of X_c became low at its earlier thickness stage (around t = 0) in Figure 4. More nitrogen, which was carried from outside, might change it.

Moreover, in many of the *SEG* cell Cs, V_{oc} increased, and I_{sc} and *FF* decreased. Since the μc-Si:H film formation was stopped before the X_c growth increases, the continuous deposition time of μc-Si:H was shortened, and much of the amorphous phase easily formed [8]. Therefore, much of the amorphous phase increased V_{oc} [3], and decreased I_{sc} [33]. Since the shunt resistance was increased by the rising number of *SEG*, *FF* was decreased [34].

The other cells (D, E) showed improved *Eff*, even when certain conditions were changed. These results showed repeatability in how the *SEG* process improves efficiency. However, variations (increase or decrease) of V_{oc}, I_{sc} and *FF* did not show the same pattern. Thus, *Eff* changed depending on each condition. This is because the solar characteristic of i-μc-Si:H are determined by the proportion of μc-Si:H and a-Si:H. As a result, the best number for *SEG* varies depending on the i-layer condition. Double *SEG* does not always produce a high *Eff*, even though it showed improvement in this experiment. The number of *SEG*s can be determined by how high X_c becomes.

5. Conclusions

It was considered that stopping the plasma-discharge of PECVD during the deposition cannot generate a high quality film, because it is likely to contain impurities. However, in this study, stopping the plasma-discharge and applying vacuum for 30 s was done a few times very consciously during the deposition. This was aimed at increasing the X_c by avoiding collisions with the neighboring grains after the film became thicker. Then, collisions of μc-Si:H with each other were suppressed. Additionally, *SEG* improved the quality of the μc-Si:H film by increasing the amorphous component.

Finally, the X_c value of holistic μc-Si:H became high. As a result, *Eff* improved by 1.3% (0.14 points), compared with the normal-condition cell. This cell used the *SEG* process several times during the deposition of i-μc-Si:H. The optimal number of *SEG* applications depends on the conditions of the μc-Si:H film. It should be determined by how high X_c becomes. *SEG* is a process that involves simply stopping the plasma discharge of VHF PECVD. It is an easily applied process, the only difference being that the process time is a few minutes longer.

References

1. Cuony, P.; Marending, M.; Alexander, D.T.L.; Boccard, M.; Bugnon, G.; Despeisse, M.; Ballif, C. Mixed-phase p-type silicon oxide containing silicon nanocrystals and its role in thin film silicon solar cells. *Appl. Phys. Lett.* **2010**, *97*, 213502. [CrossRef]

2. Naruse, Y.; Matsumoto, M.; Sekimoto, T.; Hishida, M.; Aya, Y.; Shinohara, W.; Fukushima, A.; Yata, S.; Terakawa, A.; Iseki, M.; *et al.* Identification of defective regions in thin-film Si solar cells for new-generation energy devices. In Proceedings of the 38th IEEE Photovoltaic Specialists Conference, Austin, TX, USA, 3–8 June 2012; pp. 003118–003123.

3. Bailat, J.; Domine, D.; Schluchter, R.; Steinhauser, J.; Fay, S.; Freitas, F.; Bucher, C.; Feitknecht, L.; Niquille, X.; Tscharner, T.; *et al.* High-Efficiency P-I-N Microcrystalline and Micromorph Thin Film Silicon Solar Cells Deposited on LPCVD Zno Coated Glass Substrates. In Proceedings of the 4th World Conference Photovoltaic Energy Conversion, Waikoloa, HI, USA, 7–12 May 2006; Volume 2, pp. 1533–1536.

4. Boccard, M.; Despeisse, M.; Escarre, J.; Niquille, X.; Bugnon, G.; Hanni, S.; Eymard, M.B.; Meillaud, F.; Ballif, C. High-Stable-Efficiency Tandem Thin-Film Silicon Solar Cell With Low-Refractive-Index Silicon-Oxide Interlayer. *IEEE J. Photovolt.* **2014**, *4*, 1368–1373. [CrossRef]

5. Matsui, T.; Bidiville, A.; Maejima, K.; Sai, H.; Koida, T.; Suezaki, T.; Matsumoto, M.; Saito, K.; Yoshida, I.; Kondo, M. High-efficiency amorphous silicon solar cells: Impact of deposition rate on metastability. *Appl. Phys. Lett.* **2015**, *106*, 053901. [CrossRef]

6. Python, M.; Madani, O.; Dominé, D.; Meillaud, F.; Vallat-Sauvain, E.; Ballif, C. Influence of the substrate geometrical parameter son microcrystalline silicon growth for thin-film solar cells. *Sol. Energy Mater. Sol. Cells* **2009**, *93*, 1714–1720. [CrossRef]

7. Despeisse, M.; Bugnon, G.; Feltrin, A.; Stueckelberger, M.; Cuony, P.; Meillaud, F.; Billet, A.; Ballif, C. Resistive interlayer for improved performance of thin film silicon solar cells on highly textured substrate. *Appl. Phys. Lett.* **2010**, *96*, 073507. [CrossRef]

8. Hishida, M.; Ueno, H.; Sekimoto, T.; Terakawa, A. Use of microcrystallinity depth profiling in an actual tandem silicon solar cell by polishing to achieve high conversion efficiency. *Jpn. J. Appl. Phys.* **2015**, *54*, 052302. [CrossRef]

9. Das, U.; Morrison, S.; Centurioni, E.; Madan, A. Thin film silicon materials and solar cells grown by pulsed PECVD technique. *IEE Proc. Circuits Devices Syst.* **2003**, *150*, 282–286. [CrossRef]

10. Choong, G.; Vallat-Sauvain, E.; Multone, X.; Fesquet, L.; Kroll, U.; Meier, J. Measurements of Raman crystallinity profiles in thin-film microcrystalline silicon solar cells. *J. Phys.* **2013**, *46*, 235105. [CrossRef]

11. Kimura, H.; Maeda, H.; Murakami, H.; Nakahigashi, T.; Ohtani, S.; Tabata, T.; Hayashi, T.; Kobayashi, M.; Mitsuda, Y.; Nakamura, N.; *et al.* Study of Deposition Process in Modulated RF Silane Plasma. *Jpn. J. Appl. Phys.* **1994**, *33*, 4389–4394. [CrossRef]

12. Kondo, M.; Fujiwara, H.; Matsuda, A. Fundamental aspects of low-temperature growth of microcrystalline silicon. *Thin Solid Films* **2003**, *430*, 130–134. [CrossRef]

13. Matsui, T.; Kondo, M. Advanced materials processing for high-efficiency thin-film silicon solar cells. *Sol. Energy Mater. Sol. Cells* **2013**, *119*, 156–162. [CrossRef]

14. Urbain, F.; Smirnov, V.; Becker, J.-P.; Rau, U.; Finger, F.; Ziegler, J.; Kaiser, B.; Jaegermann, W. a-Si:H/μc-Si:H tandem junction based photocathodes with high open-circuit voltage for efficient hydrogen production. *J. Mater. Res.* **2014**, *29*, 2605–2614. [CrossRef]

15. Terakawa, A. Review of thin-film silicon deposition techniques for high-efficiency solar cells developed at Panasonic/Sanyo. *Sol. Energy Mater. Sol. Cells* **2013**, *119*, 204–208. [CrossRef]

16. Kilper, T.; Beyer, W.; Bräuer, G.; Bronger, T.; Carius, R.; van den Donker, M.N.; Hrunski, D.; Lambertz, A.; Merdzhanova, T.; Mück, A.; *et al*. Oxygen and nitrogen impurities in microcrystalline silicon deposited under optimized conditions: Influence on material properties and solar cell performance. *J. Appl. Phys.* **2009**, *105*, 074509. [CrossRef]

17. Droz, C.; Vallat-Sauvain, E.; Bailat, J.; Feitknecht, L.; Meier, J.; Shah, A. Relationship between Raman crystallinity and open-circuit voltage in microcrystalline silicon solar cells. *Sol. Energy Mater. Sol. Cells* **2004**, *81*, 61–71. [CrossRef]

18. Matsui, T.; Tsukiji, M.; Saika, H.; Toyama, T.; Okamoto, H. Correlation between Microstructure and Photovoltaic Performance of Polycrystalline Silicon Thin Film Solar Cells. *Jpn. J. Appl. Phys.* **2002**, *41*, 20–27. [CrossRef]

19. Mirabella, F.M., Jr. *Internal Reflection Spectroscopy: Theory and Applications*; Mirabella, F.M., Ed.; Marcel Dekker, Inc.: New York, NY, USA, 1993.

20. Smets, A.H.M.; Matsui, T.; Kondo, M. High-rate deposition of microcrystalline silicon p-i-n solar cells in the high pressure depletion regime. *J. Appl. Phys.* **2008**, *104*, 034508. [CrossRef]

21. Smets, A.H.M.; Matsui, T.; Kondo, M. Infrared analysis of the bulk silicon-hydrogen bonds as an optimization tool for high-rate deposition of microcrystalline silicon solar cells. *Appl. Phys. Lett.* **2008**, *92*, 033506. [CrossRef]

22. Smets, A.H.M.; Matsui, T.; Kondo, M.; van de Sanden, M.C.M. The hydride stretching modes of hydrogenated vacancies in amorphous and nanocrystalline silicon: A helpful tool for material characterization. In Proceedings of the 34th IEEE Photovoltaic Specialists Conference, Philadelphia, PA, USA, 7–12 June 2009; pp. 721–724.

23. Yamashita, K.; Minami, S. Evaluation of Numerical Filters for Smoothing Spectroscopic Data. *Jpn. J. Appl. Phys.* **1969**, *8*, 1505–1512. [CrossRef]

24. Quach, N.T.; Reif, R. Solid phase epitaxy of polycrystalline silicon films: Effects of ion implantation damage. *Appl. Phys. Lett.* **1984**, *45*, 910–912. [CrossRef]

25. Kondo, M.; Fukawa, M.; Guo, L.; Matsuda, A. High rate growth of microcrystalline silicon at low temperatures. *J. Non-Cryst. Solids* **2000**, *266–269*, 84–89. [CrossRef]

26. Xu, L.; Li, Z.P.; Wen, C.; Shen, W.Z. Bonded hydrogen in nanocrystalline silicon photovoltaic materials: Impact on structure and defect density. *J. Appl. Phys.* **2011**, *110*, 064315. [CrossRef]

27. Wen, C.; Xu, H.; He, W.; Li, Z.; Shen, W. Tuning oxygen impurities and microstructure of nanocrystalline silicon photovoltaic materials through hydrogen dilution. *Nanoscale Res. Lett.* **2014**, *9*. [CrossRef] [PubMed]

28. Ehara, T. The crystalline properties of nitrogen doped hydrogenated microcrystalline silicon thin films. *Thin Solid Films* **1997**, *310*, 322–326. [CrossRef]

29. Akiharu, M.; Minoru, M.; Masahiro, Y.; Minoru, K.; Tatsuo, S. Effect of Reduction in Impurity Content for a-Si:H Films. *Appl. Phys. Lett.* **1991**, *59*, 2130.

30. Keppner, H.; Meier, J.; Torres, P.; Fischer, D.; Shah, A. Microcrystalline silicon and micromorph tandem solar cells. *J. Appl. Phys.* **1999**, *69*, 169–177. [CrossRef]

31. Sakai, H.; Yoshida, T.; Hama, T.; Ichikawa, Y. Effects of Surface Morphology of Transparent Electrode on the Open-Circuit Voltage in a-Si:H Solar Cells. *Jpn. J. Appl. Phys.* **1990**, *29*, 630–635. [CrossRef]

32. Lambertz, A.; Grundler, T.; Finger, F. Hydrogenated amorphous silicon oxide containing a microcrystalline silicon phase and usage as an intermediate reflector in thin-film silicon solar cells. *J. Appl. Phys.* **2011**, *109*, 113109. [CrossRef]

33. Flikweert, A.J.; Zimmermann, T.; Merdzhanova, T.; Weigand, D.; Appenzeller, W.; Gordijn, A. Microcrystalline thin-film solar cell deposition on moving substrates using a linear VHF-PECVD reactor and a cross-flow geometry. *J. Phys. D* **2012**, *45*, 015101. [CrossRef]

34. Meillaud, F.; Shah, A.; Bailat, J.; Vallat-Sauvain, E.; Roschek, T.; Rech, B.; Dominé, D.; Söderström, T.; Python, M.; Ballif, C. Microcrystalline silicon solar cells: Theory and diagnostic tools. In Proceedings of the 4th World Conference Photovoltaic Energy Conversion, Waikoloa, HI, USA, 7–12 May 2006; pp. 1572–1575.